Insights on the crustal evolution of the West African Craton from Hf isotopes in detrital zircons from the Anti-Atlas belt

Jacobo Abati[a,*], Abdel Mohsine Aghzer[b,1], Axel Gerdes[c,d,2], Nasser Ennih[b]

[a] Departamento de Petrología y Geoquímica and Instituto de Geología Económica, Universidad Complutense/Consejo Superior de Investigaciones Científicas, 28040 Madrid, Spain
[b] Departament Géologie, Faculte des Sciences, Université Chouaib Doukkali, El Jadida, Morocco
[c] Institut für Geowissenschaften, Mineralogie, Goethe-University Frankfurt (GUF), Altenhöferallee 1, D-60438 Frankfurt am Main, Germany
[d] Department of Earth Sciences, Stellenbosch University, Private Bag X1, Matieland 7602, South Africa

Keywords:
Anti-Atlas belt
Morocco
Hf isotopes
Detrital zircon
Crustal evolution

ABSTRACT

The Lu-Hf isotopic composition of detrital zircons has been used to investigate the crustal evolution of the northern part of the West African Craton (WAC). The zircons were separated from six samples of siliciclastic sedimentary rocks from the main Neoproterozic stratigraphic units of the Anti-Atlas belt, from the Sirwa and Zenaga inliers. The data suggest that the north part of the WAC formed during three cycles of juvenile crust formation with variable amount of reworking of older crust. The younger group of zircons, with a main population clustering around 610 Ma, has a predominant juvenile character and evidences of moderate mixing with Paleoproterozoic and Neoarchean crust, which supports that most igneous and metamorphic rocks where zircons originally crystallized were formed in an ensialic magmatic arc environment. The group of zircons in the age range 1.79–2.3 Ga corresponds to the major crust forming event in the WAC: the Eburnian orogeny. The isotopic data indicate that the provenance area should represent a crustal domain that was separated from a mantle reservoir at ~2050–2300 Ma, and further evolved with a time-integrated $^{176}Lu/^{177}Hf$ of ~0.01, characteristic of continental crust. The evolution of the Eburnian orogeny is, consequently, compatible with new crust formation in an island arc environment, the transition to a continental arc setting and a final continent–continent collision. The Lower Paleoproterozoic and Neoarchean evolution (2.3–2.75 Ga) includes a group of detrital zircon ages that has not been identified up to now in the igneous or metamorphic rocks of the north WAC basement. Their Hf isotopic signature points to reworking of mainly juvenile Neoarchean crust with some Meso- to Palaearchean contributions. The significance of these ages is uncertain: they can represent a tectonothermal event not discovered yet in the Reguibat Shield or the zircons can be far traveled from an unknown source.

1. Introduction

Lu-Hf isotopic investigations in single zircon grains of known age provides valuable information about the formation and evolution of the continental crust. Deviation of the Hf isotopic composition of one sample from the chondritic uniform reservoir (CHUR), usually reported as epsilon units, is a sensitive indicator of the source of the magmas where zircons formed, providing an estimation of the relative influence of the different components involved in the melting. Essentially, these components are juvenile depleted mantle, reworked old crust or a mixing of both. With the increasing availability and improved precision of analytical techniques, especially *in situ* zircon analyses, the Hf isotopic signature combined with the U-Pb age obtained in detrital or magmatic zircon grains has been widely used to constrain the mantle differentiation, crustal growth events and the nature of crustal reworking in many cratonic domains (Patchett et al., 1982; Stevenson and Patchett, 1990; Amelin et al., 2000; Andersen et al., 2002; Griffin et al., 2004; Zhang et al., 2006; Gerdes and Zeh, 2006; Nebel-Jacobsen et al., 2010; Morag et al., 2011). In this study we present LA-ICP-MS Lu-Hf analyses of detrital zircons from six samples of Neoproterozoic sedimentary rocks from the Pan-African Anti-Atlas belt of southern Morocco, to investigate the crustal evolution of their proposed source area, in the northern part of the West African Craton (WAC). The old cratonic nuclei of the north part of the WAC is the Reguibat shield, formed by Paleoproterozoic and Archean components (Key et al., 2008), which is separated from the Anti-Atlas belt, more to the

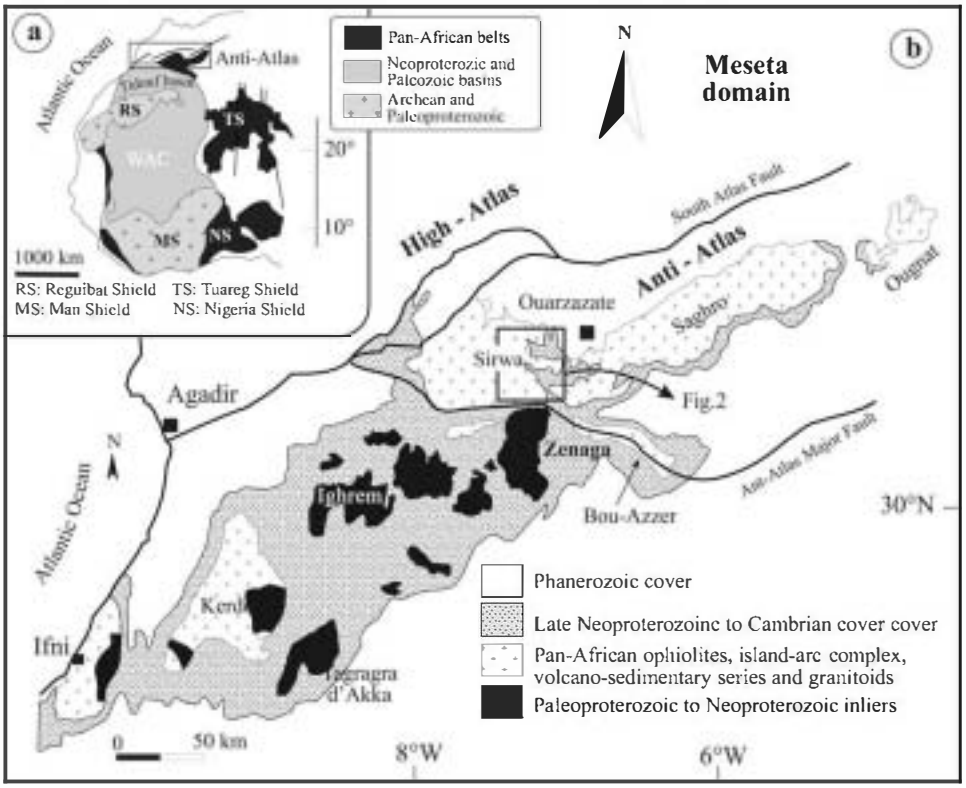

Fig. 1. (a) Scheme of the cratonic areas, basins and the peripheral Pan-African belts of the West African Craton. (b) Geological sketch map of the Anti-Atlas belt in southern Morocco.
Based on Abati et al. (2010).

north, by the Tindouf basin (Fig. 1). The Anti-Atlas represents the remobilization of the northern cratonic boundary during the Pan-African orogeny (Ennih and Liegeois, 2008), including arc accretion and ophiolite obduction to the margin. The older basement of the Anti-Atlas is formed by Paleoproterozoic Eburnian (2.0–2.2 Ga) magmatic and metamorphic rocks, covered by Neoproterozoic to Paleozoic sedimentary sequences. According to Abati et al. (2010), the major source of Neoproterozoic sediments (pre to post Pan-African) was the Reguibat shield. For that reason, the detrital zircon populations from these sedimentary rocks are probably a representative sample of the main magmatic and metamorphic rocks from the north part of the WAC, and their isotopic composition can provide information about the main crustal components involved and their evolution.

2. Geological setting

2.1. West African Craton

The available age and isotopic data indicate that the building and amalgamation of the WAC basement took place through four major orogenic cycles: (1) Leonian cycle (3.5–3.0 Ga; Rocci et al., 1991; Kröner et al., 2001; Potrel et al., 1996; Thiéblemont et al., 2004), (2) the Liberian cycle (2.95–2.75 Ga; Hurley et al., 1971; Auvray et al., 1992; Potrel et al., 1998; Key et al., 2008), (3) the Eburnian–Birimian cycle (2.2–1.75 Ga; Abouchami et al., 1990; Liégeois et al., 1991; Boher et al., 1992; Hirdes et al., 1992; Aït Malek et al., 1998; Schofield et al., 2006) and (4) the Pan-African remobilization (760–660 Ma; Leblanc and Lancelot, 1980; Saquaque et al., 1989; Hefferan et al., 2000; Thomas et al., 2002; Samson et al., 2004). One of the main characteristics of the WAC is that no Mesoproterozoic events or rocks are known, suggesting a quiescent period between 1.7 and 1.0 Ga (*e.g.* Ennih and Liegeois, 2008). The exposed parts of the craton outcrop in two main uplifts: the Reguibat shield in the north (Mauritania, Morocco and Algeria) and the Leo Shield in the south (Fig. 1).

2.2. Anti-Atlas belt

The Anti-Atlas belt of southern Morocco is located on the northern edge of the West African Craton (WAC) (Fig. 1a). It is separated in the north from the High-Atlas and the Meseta domain by the South Atlas Fault (Fig. 1b). This belt is composed essentially by: (1) Basement rocks of Paleoproterozoic age (*ca.* 2 Ga); (2) Neoproterozoic sequences with lowermost units involved in the Pan African orogeny and (3) unconformably overlying Paleozoic rocks.

The Paleoproterozoic basement and overlying Pan-African Neoproterozoic sequences outcrops in several inliers (Ifni, Tagrara d'Akka, Kerdous, Sirwa, Ighrem, Zenaga, Iguerda, Bou Azzer, *etc.*) beneath post-Pan-African collisional cover consisting of late Neoproterozoic to Cambrian rocks (Fig. 1b).

The Paleoproterozoic rocks (2030–2200 Ma) (Aït Malek et al., 1998; Thomas et al., 2002; Walsh et al., 2002) correspond to the northward margin of the WAC and consists essentially of low to high-grade metasediments intruded by calc-alkaline plutonic rocks. They have age-similarities with the West African Birimian crust.

The Neoproterozoic sequences involved in Pan-African orogeny are associated with a series of geodynamic process that summarized as follows:

1) The break-up and rifting of the northern edge of the WAC, leading to the formation of a passive margin sequence (The Taghdout Group) deposited on the Paleoproterozoic basement.

2) The creation of an oceanic basin (760–697 Ma) (Samson et al., 2004; El Hadi et al., 2010) between the northern edge of the WAC and an unknown northern terrane. The preserved relic of this oceanic crust corresponds to highly sheared allochtonous ophiolite complexes (The Bou Azzer Group).
3) A subduction phase and island-arc formation (The Iriri Group) (743 Ma) (Thomas et al., 2002). A magmatic event at 750–700 Ma (D'Lemos et al., 2006) recorded in the continental margin tectonically underlying the Taghdout Group in Bou Azzer inlier is interpreted as the result of pre-Pan-African rifting evolution (El Hadi et al., 2010) or as a continuous arc building event by Gasquet et al. (2008).
4) The ophiolite obduction, arc accretion onto the northern edge of the WAC and syn-tectonic calc-alkaline intrusions (660–635 Ma) (Thomas et al., 2002; Inglis et al., 2004; El Hadi et al., 2010).
5) A late to post-collisional Neoproterozoic evolution marked by the deposition of the Saghro Group, the Bou Salda Group and the emplacement of high-K-calc-alkaline granitoids of the Assarag suite. The Saghro Group consists of a volcanoclastic rocks metamorphosed at greenschist-facies conditions. The Bou Salda Group is a volcanosedimentary sequence that is preserved from the Pan-African metamorphism. The age of this group (620–610 Ma; Abati et al., 2010) is the same as the Saghro Group (630–610 Ma) (Abati et al., 2010) and is indistinguishable from the age of 615–579 Ma (Aït Malek et al., 1998; De Wall et al., 2001; Levresse et al., 2001; Thomas et al., 2002; Inglis et al., 2004) of some granitoid intrusions of the Assarag suite (Abati et al., 2010). This synchronicity of the sedimentation and subsequent metamorphism, deformation and intrusion by plutonic bodies is a typical feature of magmatic arc settings (Abati et al., 2003, 2010). It suggests that the Saghro and Bou Salda Groups come from the erosion dismantling of a magmatic arc located to the north of the Pan-African suture and built upon north WAC basement (Abati et al., 2010). This arc-setting model can be correlated with the late Neoproterozoic (*ca.* 640–570 Ma) long-lived arc-system characteristic of the north Gondwana margin and peri-Gondwanan terranes. The post-630–610 Ma deformation (and ante-580 Ma: age of intrusive rocks of the overlying discordant Ouarzazate Group) affecting essentially the Saghro Group corresponds to the late phase of Pan-African collision (Abati et al., 2010).

The late Neoproterozoic evolution of the Anti-Atlas belt is marked by the deposition of the volcano-sedimentary rocks of the Ouarzazate Group (577–552 Ma) (Thomas et al., 2002; Walsh et al., 2002; Gasquet et al., 2005; Abati et al., 2010) that rest unconformably on the Paleoproterozoic basement and the Neoproterozoic units involved in the Pan-African orogeny.

3. Sample description

Six sedimentary rocks were sampled from the Taghdout, Saghro, Bou Salda (Sirwa inlier) and Ouarzazate groups (Zenaga inlier), encompassing the major units of the Neoproterozoic sequences of the Anti-Atlas (Fig. 2). Following a bottom to top order, sample AA1 is an undeformed quartzite of the Mimount Formation, collected from the type locality of Taghdout village, belonging to the Taghdout Group, interpreted as the oldest rocks overlying the WAC (Thomas et al., 2002; 740–800 Ma). Three samples are from Saghro Group: AA5 is a arkose and AA3 is a conglomerate (diamictite) from the Imghi Formation, whereas AA6 is an arkosic sandstone from the Azarwas Formation. Sample AA4 is a quartzic cobble of a conglomerate from the Lmakhzane Member of the Bou Salda Group. Finally, sample AA7 is an epiclastic conglomerate of the Ouarzazate Group. The location of the samples is showed in the map and in the schematic stratigraphic column of Fig. 2. They are the same samples of the U-Pb study of Abati et al., 2010, and more detailed descriptions, maps and stratigraphic features can be found there (Table 1).

3.1. Analytical techniques

Hafnium isotope measurements were performed with Thermo-Scientific Neptune multi-collector ICP-MS coupled to a New Wave Research UP213 ultraviolet laser system at Goethe-University Frankfurt (GUF) following the method described by Gerdes and Zeh (2006, 2009). A teardrop-shaped, low volume (<2.5 cm^3) laser cell with fast response (<1 s) and low wash-out time was used (Janousek et al., 2006; Frei and Gerdes, 2009). The Lu-Hf laser spots (40 μm in diameter) were drilled on top of the 30 μm spots used for U-Pb analyses.

Data were collected in static mode during 58 s of laser ablation. Nitrogen (~0.005 l/min) was introduced *via* a Cetac Aridus into the Ar sample carrier gas to enhance sensitivity (~30%) and to reduce oxide formation. The use of the Aridus system allowed bracketing of laser ablation analyses with solution mode analyses. Analytical protocols were the same for laser ablation and solution mode analyses. The isotopes ^{172}Yb, ^{173}Yb and ^{175}Lu were simultaneously monitored during each analysis step to allow for correction of isobaric interferences of Lu and Yb isotopes on mass 176. The ^{176}Lu and ^{176}Yb were calculated using $^{176}Lu/^{175}Lu$ of 0.02658 and $^{176}Yb/^{173}Yb$ of 0.795015 (both GUF in-house values). The accuracy of the correction was tested with a 40 ppb JMC475 solution doped with natural Yb and Lu. Even at about 100% interference the corrected yielded a $^{176}Hf/^{177}Hf$ of 0.282157 ± 40 (2SD, Table S1). For a more detailed discussion see Gerdes and Zeh (2009). All data were adjusted relative to the JMC475 of $^{176}Hf/^{177}Hf$ ratio = 0.282160 and quoted uncertainties are quadratic additions of the within run precision of each analysis and the reproducibility of the JMC475 (2SD = 0.0033%, n = 8; Table S1). Accuracy and external reproducibility of the method was verified by repeated analyses of reference zircon GJ-1 and Plešovice, which yielded a $^{176}Hf/^{177}Hf$ of 0.282003 ± 0.000023 (2SD, n = 23) and of 0.282469 ± 0.000023 (n = 15), respectively (Table S1).

4. Hf isotopes and WAC crustal evolution

The detrital zircons of this study can be grouped in two major age populations (Fig. 3a), pointing to the existence of two periods of maximum granitoid production: a younger Neoproterozoic group ranging from 540 to 750 Ma (syn to post Pan-African collision) and an older Paleoproterozoic to Archean group ranging from 1790 to 2750 Ma. The two groups are separated by an age gap between 1.7 and 0.8 Ma, characteristic of the WAC (Ennih and Liegeois, 2008). The older group can in turn be separated in two different groups, according to their isotopic features (1790–2300 and 2300–2750 Ma).

4.1. Neoproterozoic zircons: a pan-african arc in the periphery of gondwana?

The zircons show a wide variability of the initial epsilon Hf (εHf_i) values, ranging between −14 and 14 (Fig. 3a and b). From the 111 zircons analyzed of this age range, about 70% have positive εHf_i, indicating that they were crystallized either from magmas directly derived from a depleted mantle source (=juvenile magmas) contaminated with different amounts of older crust or by partial melting of a relatively juvenile crust, *e.g.* a recently formed island arc. In any case, the data suggest that significant amounts of juvenile crust were formed during late Neoproterozoic time. The

Table 1
Lu-Hf isotopic data.

	$^{176}Yb/^{177}Hf$ [a]	±2σ	$^{176}Lu/^{177}Hf$ [a]	±2σ	$^{178}Hf/^{177}Hf$	$^{180}Hf/^{177}Hf$	Sig_{Hf} [b] (V)	$^{176}Hf/^{177}Hf$ [d]	±2σ [c]	$^{176}Hf/^{177}Hf_{(t)}$	εHf(t) [d]	±2σ [c]	T_{DM2} [e] (Ga)	Age [f] (Ma)	±2σ
AA1_1	0.0296	48	0.00112	14	1.46730	1.88686	14	0.281581	28	0.281534	5.7	1.0	2.19	2202	17
AA1_2	0.0312	35	0.00088	9	1.46734	1.88680	13	0.281626	25	0.281590	6.4	0.9	2.11	2149	12
AA1_3	0.0427	47	0.00112	11	1.46733	1.88687	12	0.281628	27	0.281583	4.8	1.0	2.15	2091	21
AA1_5	0.0323	31	0.00087	7	1.46711	1.88656	16	0.281670	33	0.281636	6.2	1.2	2.05	2069	34
AA1_6	0.0223	22	0.00063	5	1.46733	1.88671	16	0.281551	22	0.281528	−0.9	0.8	2.33	1927	27
AA1_7	0.0164	39	0.00047	10	1.46739	1.88670	19	0.281621	21	0.281601	8.0	0.8	2.06	2200	29
AA1_9	0.0212	18	0.00058	4	1.46717	1.88651	13	0.281431	24	0.281407	1.2	0.8	2.44	2206	16
AA1_11	0.0772	143	0.00205	39	1.46736	1.88685	21	0.281668	41	0.281587	4.7	1.5	2.14	2079	12
AA1_12	0.0632	120	0.00185	33	1.46729	1.88682	18	0.281681	50	0.281604	7.6	1.8	2.06	2178	23
AA1_16	0.0107	13	0.00035	3	1.46721	1.88665	20	0.281329	16	0.281313	2.9	0.6	2.52	2420	30
AA1_17	0.0485	77	0.00145	21	1.46733	1.88677	13	0.281392	33	0.281331	−1.6	1.2	2.59	2199	24
AA1_18	0.0385	43	0.00109	12	1.46734	1.88672	14	0.280991	27	0.280933	−3.0	1.0	3.11	2746	30
AA1_20	0.0294	25	0.00090	6	1.46733	1.88687	14	0.281514	30	0.281479	0.7	1.1	2.36	2075	26
AA1_27	0.0124	10	0.00036	2	1.46718	1.88658	13	0.281648	21	0.281634	6.3	0.8	2.05	2077	24
AA1_28	0.0200	19	0.00054	4	1.46721	1.88671	13	0.281354	28	0.281328	4.4	1.0	2.47	2462	19
AA1_30	0.0205	20	0.00051	4	1.46731	1.88677	13	0.281580	19	0.281557	8.4	0.7	2.11	2283	27
AA1_32	0.0271	37	0.00074	8	1.46724	1.88679	14	0.281288	25	0.281253	2.9	0.9	2.60	2514	16
AA1_33	0.0635	117	0.00147	23	1.46722	1.88653	15	0.281652	39	0.281593	5.1	1.4	2.13	2087	13
AA1_37	0.0201	29	0.00048	7	1.46730	1.88689	17	0.281600	18	0.281583	1.5	0.6	2.21	1948	11
AA1_41	0.0238	25	0.00075	6	1.46714	1.88650	16	0.281537	21	0.281507	2.3	0.8	2.29	2100	16
AA1_42	0.0159	13	0.00043	3	1.46724	1.88672	13	0.281204	20	0.281186	−6.6	0.7	2.87	2205	26
AA1_43	0.0262	21	0.00074	5	1.46724	1.88681	14	0.281404	21	0.281371	3.2	0.8	2.44	2343	14
AA1_45	0.0496	50	0.00156	17	1.46733	1.88682	19	0.281480	27	0.281411	4.0	1.0	2.38	2319	22
AA1_46	0.0410	34	0.00113	8	1.46731	1.88676	17	0.281647	26	0.281603	4.7	0.9	2.12	2055	18
AA1_47	0.0081	11	0.00020	3	1.46731	1.88689	19	0.281486	20	0.281478	0.8	0.7	2.36	2080	17
AA1_52	0.0102	10	0.00030	2	1.46717	1.88648	15	0.281287	18	0.281273	1.7	0.7	2.60	2432	33
AA1_55	0.0230	20	0.00081	6	1.46715	1.88663	13	0.281591	20	0.281562	−0.2	0.7	2.27	1905	29
AA1_57	0.0222	20	0.00060	4	1.46731	1.88687	14	0.281599	20	0.281576	2.6	0.7	2.20	2006	27
AA1_58	0.0334	28	0.00084	5	1.46722	1.88654	13	0.281386	24	0.281346	4.6	0.8	2.45	2443	20
AA1_60	0.0168	14	0.00045	3	1.46733	1.88687	14	0.281527	18	0.281511	−3.1	0.6	2.40	1857	24
AA1_61	0.0688	66	0.00166	14	1.46718	1.88656	17	0.281484	37	0.281418	−0.7	1.3	2.47	2105	17
AA1_64	0.0697	60	0.00162	10	1.46719	1.88652	19	0.281092	38	0.281030	−16.3	1.3	3.26	2028	14
AA1_65	0.0205	18	0.00051	3	1.46730	1.88668	13	0.281651	18	0.281623	26.0	0.7	1.64	2936	15
AA1_66	0.0389	73	0.00105	23	1.46733	1.88677	14	0.281096	27	0.281055	−13.8	1.0	3.18	2096	16
AA1_70	0.0346	35	0.00083	6	1.46715	1.88649	13	0.281666	23	0.281634	4.8	0.8	2.08	2013	19
AA1_72	0.0670	66	0.00169	15	1.46732	1.88679	17	0.281685	33	0.281618	6.0	1.2	2.08	2090	19
AA1_73	0.0668	71	0.00180	19	1.46717	1.88647	15	0.281468	26	0.281392	1.0	0.9	2.46	2220	23
AA1_74	0.0471	46	0.00119	8	1.46716	1.88658	12	0.281604	26	0.281557	3.6	0.9	2.21	2077	23
AA1_80	0.0331	28	0.00082	6	1.46725	1.88683	16	0.281229	21	0.281196	−8.5	0.8	2.90	2110	19
AA1_81	0.0755	67	0.00187	15	1.46725	1.88662	19	0.281700	36	0.281628	4.8	1.3	2.09	2021	10
AA1_84	0.0245	22	0.00061	4	1.46713	1.88656	17	0.281612	24	0.281589	3.4	0.8	2.17	2020	15
AA1_87	0.0428	58	0.00095	15	1.46712	1.88658	15	0.281114	34	0.281076	−12.8	1.2	3.13	2108	20
AA1_89	0.0476	52	0.00130	10	1.46735	1.88676	12	0.281200	29	0.281137	−0.6	1.0	2.81	2538	13
AA1_90	0.0739	72	0.00186	13	1.46719	1.88656	19	0.281397	38	0.281324	−5.0	1.4	2.67	2064	11
AA1_93	0.0255	21	0.00067	5	1.46719	1.88657	15	0.281566	20	0.281539	3.6	0.7	2.23	2105	19
AA1_97	0.0232	27	0.00062	5	1.46718	1.88657	17	0.281267	20	0.281238	2.7	0.7	2.62	2527	15
AA1_104	0.0031	13	0.00007	3	1.46723	1.88682	15	0.281361	15	0.281358	−3.3	0.5	2.59	2087	13
AA1_106	0.0031	13	0.00007	3	1.46723	1.88682	15	0.281361	15	0.281358	−2.3	0.5	2.57	2129	11
AA1_109	0.0493	42	0.00120	8	1.46726	1.88667	12	0.281580	30	0.281539	−3.3	1.1	2.36	1809	15
AA1_110	0.0203	22	0.00059	6	1.46734	1.88684	16	0.281041	20	0.281011	−4.6	0.7	3.05	2561	10
AA1_111	0.0153	17	0.00051	4	1.46731	1.88663	14	0.281380	23	0.281358	2.2	0.8	2.48	2322	12
AA1_116	0.0372	33	0.00106	7	1.46724	1.88673	16	0.281364	27	0.281315	2.3	1.0	2.53	2392	9
AA1_120	0.0204	17	0.00062	5	1.46729	1.88686	14	0.281304	22	0.281274	3.7	0.8	2.55	2513	10
AA1_125	0.0247	20	0.00069	4	1.46727	1.88677	11	0.281529	26	0.281504	−0.8	0.9	2.36	1969	30
AA1_127	0.0436	40	0.00105	9	1.46723	1.88667	9	0.281502	31	0.281465	−5.5	1.1	2.50	1825	15

Table 1 (*Continued*)

	$^{176}Yb/^{177}Hf$ [a]	±2σ	$^{176}Lu/^{177}Hf$ [a]	±2σ	$^{178}Hf/^{177}Hf$	$^{180}Hf/^{177}Hf$	Sig_{Hf} [b] (V)	$^{176}Hf/^{177}Hf$ [d]	±2σ [c]	$^{176}Hf/^{177}Hf_{(t)}$	εHf(t) [d]	±2σ [c]	T_{DM2} [e] (Ga)	Age [f] (Ma)	±2σ
AA3_1	0.0190	16	0.00053	4	1.46718	1.88648	12	0.282072	20	0.282066	−11.9	0.7	1.85	608	9
AA3_3	0.0798	76	0.00194	14	1.46729	1.88676	14	0.282347	27	0.282326	−3.3	1.0	1.36	579	9
AA3_5	0.0360	51	0.00094	12	1.46720	1.88683	15	0.282199	25	0.282189	−7.8	0.9	1.62	598	9
AA3_7	0.0305	34	0.00085	9	1.46721	1.88652	12	0.281610	21	0.281579	0.4	0.7	2.24	1905	26
AA3_12	0.0245	20	0.00064	4	1.46715	1.88660	13	0.281665	20	0.281640	7.3	0.7	2.03	2111	17
AA3_14	0.0504	41	0.00122	7	1.46726	1.88679	15	0.282307	28	0.282292	−3.3	1.0	1.40	633	9
AA3_15	0.0447	37	0.00113	8	1.46720	1.88653	11	0.281180	27	0.281121	3.1	1.0	2.75	2722	14
AA3_16	0.0431	35	0.00109	7	1.46723	1.88673	15	0.282316	26	0.282303	−3.4	0.9	1.39	612	10
AA3_17	0.0827	84	0.00187	13	1.46723	1.88666	15	0.282291	43	0.282270	−4.8	1.5	1.46	603	11
AA3_18	0.0503	48	0.00130	10	1.46719	1.88657	11	0.281634	30	0.281582	5.1	1.1	2.14	2106	14
AA3_19	0.0335	28	0.00082	5	1.46720	1.88658	16	0.282070	21	0.282061	−11.3	0.8	1.85	640	8
AA3_20	0.0700	88	0.00161	16	1.46724	1.88655	13	0.281714	38	0.281658	1.5	1.4	2.12	1830	34
AA3_21	0.0223	22	0.00066	6	1.46724	1.88661	15	0.281627	21	0.281600	7.3	0.8	2.07	2173	19
AA3_23	0.0265	23	0.00073	6	1.46729	1.88673	13	0.281616	21	0.281588	3.3	0.7	2.17	2016	15
AA3_24	0.0546	48	0.00140	10	1.46728	1.88672	15	0.281629	30	0.281573	4.2	1.1	2.17	2080	17
AA3_26	0.0517	52	0.00132	12	1.46719	1.88679	14	0.281637	31	0.281584	4.7	1.1	2.15	2085	15
AA3_27	0.1133	95	0.00281	18	1.46715	1.88654	11	0.282352	55	0.282317	−2.2	2.0	1.35	644	11
AA3_28	0.0549	88	0.00135	19	1.46720	1.88663	13	0.281655	31	0.281603	4.7	1.1	2.13	2056	10
AA3_29	0.0256	22	0.00062	4	1.46713	1.88650	16	0.281588	22	0.281566	−0.1	0.8	2.27	1907	13
AA3_31	0.0178	18	0.00054	4	1.46721	1.88662	15	0.281579	19	0.281558	4.8	0.7	2.18	2128	10
AA3_35	0.0166	13	0.00043	3	1.46718	1.88670	12	0.281125	20	0.281105	−5.6	0.7	2.95	2374	21
AA3_36	0.0164	14	0.00049	3	1.46715	1.88650	14	0.282554	16	0.282548	6.4	0.6	0.89	662	12
AA3_37	0.0399	34	0.00105	6	1.46712	1.88652	12	0.282341	28	0.282329	−2.9	1.0	1.35	593	10
AA3_38	0.0700	60	0.00161	10	1.46722	1.88663	12	0.282325	35	0.282306	−3.0	1.2	1.38	624	12
AA3_39	0.0845	79	0.00196	14	1.46722	1.88659	13	0.282292	41	0.282270	−4.6	1.5	1.45	612	12
AA3_40	0.0365	34	0.00090	7	1.46721	1.88657	11	0.282290	24	0.282280	−4.3	0.9	1.43	611	11
AA3_41	0.0525	118	0.00126	27	1.46721	1.88662	13	0.282291	37	0.282276	−3.8	1.3	1.43	637	11
AA3_43	0.0345	30	0.00104	7	1.46719	1.88651	13	0.282544	23	0.282532	4.8	0.8	0.94	613	10
AA3_44	0.0483	50	0.00132	11	1.46723	1.88667	11	0.281567	29	0.281512	4.7	1.0	2.24	2193	19
AA3_46	0.0797	68	0.00190	13	1.46728	1.88677	13	0.282309	37	0.282286	−3.4	1.3	1.41	637	13
AA3_49	0.0537	62	0.00137	12	1.46720	1.88664	8	0.282312	30	0.282296	−3.5	1.0	1.40	617	10
AA3_50	0.0747	66	0.00175	12	1.46720	1.88655	13	0.282323	39	0.282304	−3.9	1.4	1.40	591	9
AA3_51	0.1180	107	0.00266	18	1.46714	1.88659	10	0.282503	53	0.282471	3.1	1.9	1.05	634	11
AA3_57	0.0714	59	0.00176	11	1.46731	1.88682	16	0.281604	33	0.281534	2.8	1.2	2.25	2078	12
AA3_58	0.0822	71	0.00214	15	1.46731	1.88684	13	0.282716	37	0.282688	12.5	1.3	0.59	714	12
AA3_62	0.0461	44	0.00115	8	1.46719	1.88655	14	0.282310	27	0.282297	−4.1	0.9	1.41	591	12
AA3_66	0.0919	80	0.00202	13	1.46724	1.88681	12	0.282434	44	0.282411	0.3	1.6	1.18	606	11
AA3_67	0.0950	90	0.00224	17	1.46722	1.88679	12	0.282301	44	0.282275	−4.3	1.6	1.44	618	11
AA3_69	0.0255	21	0.00073	5	1.46733	1.88665	13	0.282680	23	0.282672	9.8	0.8	0.66	616	12
AA3_73	0.1112	91	0.00264	17	1.46719	1.88673	10	0.282387	49	0.282358	−1.8	1.7	1.29	598	11
AA3_75	0.0320	26	0.00083	5	1.46716	1.88656	14	0.281617	21	0.281585	2.1	0.8	2.20	1970	19
AA3_77	0.0318	37	0.00078	8	1.46716	1.88650	16	0.281386	22	0.281353	−0.3	0.8	2.54	2221	16
AA3_78	0.0289	23	0.00074	4	1.46730	1.88662	13	0.281582	21	0.281549	8.2	0.7	2.12	2289	20
AA3_82	0.0360	31	0.00086	5	1.46715	1.88648	11	0.281249	21	0.281208	1.4	0.7	2.68	2515	9
AA3_85	0.0231	20	0.00060	4	1.46718	1.88657	12	0.281541	21	0.281517	2.4	0.7	2.28	2087	23
AA3_86	0.0445	51	0.00111	12	1.46718	1.88678	12	0.282202	28	0.282189	−7.5	1.0	1.61	610	10
AA3_87	0.0231	25	0.00059	5	1.46730	1.88676	13	0.281557	22	0.281534	−0.1	0.8	2.31	1955	18
AA3_88	0.0160	13	0.00040	3	1.46718	1.88655	12	0.281593	18	0.281580	−2.1	0.6	2.29	1795	23
AA3_91	0.0471	55	0.00117	13	1.46736	1.88692	12	0.281386	24	0.281335	0.0	0.9	2.55	2261	13
AA3_93	0.1673	411	0.00299	67	1.46718	1.88648	12	0.281406	74	0.281266	2.0	2.6	2.60	2454	14
AA3_97	0.1173	97	0.00283	17	1.46731	1.88679	14	0.282277	53	0.282241	−4.5	1.9	1.49	661	12
AA3_100	0.0344	34	0.00103	8	1.46714	1.88649	16	0.282553	25	0.282541	5.1	0.9	0.92	616	8
AA3_110	0.0236	20	0.00069	4	1.46724	1.88680	15	0.281594	20	0.281566	5.9	0.7	2.15	2166	16
AA3_112	0.0733	61	0.00183	12	1.46718	1.88653	15	0.282289	32	0.282268	−4.6	1.1	1.46	614	10
AA3_115	0.0147	13	0.00042	3	1.46713	1.88644	13	0.281640	20	0.281623	4.9	0.7	2.10	2031	16
AA3_124	0.0672	55	0.00166	11	1.46725	1.88685	16	0.282289	32	0.282270	−4.6	1.1	1.45	610	13

Table 1 (*Continued*)

	$^{176}Yb/^{177}Hf$[a]	±2σ	$^{176}Lu/^{177}Hf$[a]	±2σ	$^{178}Hf/^{177}Hf$	$^{180}Hf/^{177}Hf$	Sig_{Hf}[b] (V)	$^{176}Hf/^{177}Hf$[d]	±2σ[c]	$^{176}Hf/^{177}Hf_{(t)}$	εHf(t)[d]	±2σ[c]	T_{DM2}[e] (Ga)	Age[f] (Ma)	±2σ
AA3_125	0.0614	71	0.00165	14	1.46718	1.88664	17	0.281616	42	0.281559	−3.0	1.5	2.33	1789	22
AA4_6	0.0160	15	0.00050	5	1.46736	1.88684	12	0.281438	17	0.281417	1.9	0.6	2.41	2218	21
AA4_7	0.0242	19	0.00083	6	1.46734	1.88692	21	0.281471	18	0.281441	−4.1	0.6	2.50	1923	13
AA4_9	0.0321	28	0.00093	9	1.46725	1.88675	17	0.281359	20	0.281320	−1.8	0.7	2.61	2210	19
AA4_10	0.0188	12	0.00057	4	1.46732	1.88691	13	0.281548	18	0.281527	−0.7	0.7	2.33	1940	14
AA4_11	0.0075	5	0.00027	2	1.46734	1.88675	12	0.281548	20	0.281537	4.1	0.7	2.22	2130	27
AA4_12	0.0431	35	0.00133	10	1.46736	1.88693	15	0.281609	27	0.281556	3.3	1.0	2.21	2066	24
AA4_13	0.0190	16	0.00055	4	1.46731	1.88681	15	0.281681	17	0.281662	1.3	0.6	2.12	1819	19
AA4_16	0.0190	16	0.00051	4	1.46725	1.88669	15	0.281333	22	0.281309	3.4	0.8	2.52	2450	13
AA4_17	0.0354	38	0.00106	15	1.46727	1.88679	19	0.281576	23	0.281535	1.7	0.8	2.27	2032	18
AA4_19	0.0272	27	0.00080	9	1.46727	1.88693	16	0.282043	19	0.282034	−12.8	0.7	1.91	616	10
AA4_20	0.0286	21	0.00086	7	1.46730	1.88676	18	0.281592	19	0.281557	3.9	0.7	2.20	2088	11
AA4_21	0.0342	28	0.00092	9	1.46713	1.88648	15	0.281435	21	0.281394	3.9	0.8	2.40	2343	28
AA4_23	0.0402	26	0.00109	7	1.46726	1.88663	13	0.281464	25	0.281418	1.4	0.9	2.42	2194	15
AA4_26	0.0095	8	0.00027	3	1.46729	1.88666	14	0.281324	19	0.281311	5.0	0.7	2.48	2516	16
AA4_29	0.0196	14	0.00065	5	1.46729	1.88664	13	0.282065	20	0.282058	−11.8	0.7	1.86	624	23
AA4_30	0.0188	13	0.00064	5	1.46734	1.88694	10	0.281598	24	0.281574	1.2	0.9	2.23	1947	17
AA4_35	0.0028	9	0.00009	3	1.46731	1.88683	18	0.281527	19	0.281523	1.9	0.7	2.28	2055	51
AA4_36	0.0150	13	0.00059	6	1.46734	1.88687	15	0.281635	19	0.281613	2.2	0.7	2.16	1934	20
AA4_42	0.0140	10	0.00056	4	1.46736	1.88694	16	0.281629	20	0.281608	3.3	0.7	2.15	1986	12
AA4_43	0.0141	9	0.00041	3	1.46723	1.88655	13	0.281313	20	0.281294	3.1	0.7	2.54	2456	22
AA4_45b	0.0306	19	0.00098	6	1.46730	1.88668	16	0.281660	23	0.281622	4.6	0.8	2.10	2021	17
AA4_47	0.0257	59	0.00080	17	1.46726	1.88689	17	0.281592	20	0.281557	7.9	0.7	2.12	2264	34
AA4_48	0.0376	24	0.00109	7	1.46736	1.88691	17	0.281271	20	0.281221	−0.4	0.7	2.70	2422	17
AA4_52	0.0242	21	0.00079	7	1.46735	1.88693	16	0.280998	21	0.280960	−6.8	0.7	3.16	2542	16
AA4_59	0.0228	14	0.00059	4	1.46724	1.88666	17	0.281626	18	0.281604	4.4	0.6	2.13	2042	14
AA4_60	0.0292	26	0.00078	7	1.46718	1.88675	13	0.281180	20	0.281143	−1.6	0.7	2.83	2487	18
AA4_66	0.0283	30	0.00085	9	1.46736	1.88694	13	0.281180	22	0.281143	−6.8	0.8	2.93	2262	27
AA4_67	0.0016	4	0.00005	1	1.46726	1.88692	17	0.281410	16	0.281407	1.0	0.6	2.44	2197	43
AA4_68	0.0557	38	0.00171	11	1.46737	1.88694	16	0.281646	27	0.281577	5.3	0.9	2.15	2120	14
AA4_69	0.0354	48	0.00093	10	1.46724	1.88684	14	0.282573	23	0.282561	7.1	0.8	0.86	671	15
AA4_70	0.0159	10	0.00045	3	1.46723	1.88662	14	0.281581	18	0.281562	7.3	0.6	2.12	2228	32
AA4_75	0.0213	25	0.00056	6	1.46721	1.88656	14	0.281633	17	0.281611	4.8	0.6	2.11	2048	24
AA4_76	0.0539	42	0.00162	14	1.46733	1.88692	12	0.281398	31	0.281330	−1.8	1.1	2.60	2192	14
AA4_78	0.0172	14	0.00045	3	1.46721	1.88670	14	0.281608	17	0.281590	4.2	0.6	2.15	2052	17
AA4_80	0.0364	26	0.00105	7	1.46714	1.88646	14	0.281603	21	0.281564	1.1	0.7	2.25	1960	13
AA4_81	0.0162	11	0.00041	3	1.46715	1.88654	14	0.281134	17	0.281114	−2.4	0.6	2.88	2497	16
AA4_83	0.0192	13	0.00050	3	1.46723	1.88678	15	0.281105	20	0.281084	−9.0	0.7	3.05	2259	77
AA4_84	0.0250	15	0.00064	4	1.46722	1.88671	15	0.281349	19	0.281320	2.4	0.7	2.52	2389	11
AA4_86	0.0275	21	0.00071	5	1.46722	1.88655	14	0.281719	19	0.281695	3.1	0.7	2.04	1847	43
AA4_88	0.0124	10	0.00030	3	1.46723	1.88657	15	0.281513	18	0.281502	−2.3	0.6	2.39	1908	17
AA4_90	0.0165	11	0.00047	3	1.46718	1.88659	15	0.281337	16	0.281315	3.6	0.6	2.51	2448	18
AA5_2	0.0295	22	0.00096	6	1.46721	1.88676	13	0.282680	24	0.282669	10.0	0.9	0.66	633	11
AA5_5	0.0276	25	0.00083	7	1.46717	1.88651	13	0.282582	18	0.282573	6.0	0.6	0.86	607	11
AA5_7	0.0238	18	0.00066	4	1.46718	1.88665	13	0.281612	22	0.281585	6.6	0.8	2.11	2164	69
AA5_8	0.0199	14	0.00058	5	1.46737	1.88692	18	0.281613	16	0.281593	−1.1	0.6	2.25	1819	13
AA5_10	0.0496	34	0.00152	12	1.46724	1.88668	15	0.282521	27	0.282504	3.2	0.9	1.00	590	12
AA5_11	0.0198	21	0.00060	6	1.46734	1.88676	16	0.282459	19	0.282452	1.6	0.7	1.10	601	11
AA5_17	0.0242	33	0.00086	11	1.46736	1.88692	14	0.281593	20	0.281556	6.8	0.7	2.14	2215	24
AA5_18	0.0225	14	0.00060	4	1.46721	1.88675	15	0.281420	19	0.281395	−1.2	0.7	2.50	2119	22
AA5_19	0.0449	31	0.00145	9	1.46726	1.88669	15	0.282583	28	0.282567	5.4	1.0	0.88	588	10
AA5_24	0.0744	67	0.00198	16	1.46716	1.88644	13	0.282611	34	0.282590	6.1	1.2	0.84	582	12
AA5_26	0.0156	11	0.00050	3	1.46722	1.88664	18	0.282665	18	0.282658	11.1	0.6	0.66	695	14
AA5_32	0.0207	28	0.00063	6	1.46717	1.88654	16	0.282658	18	0.282651	9.2	0.6	0.70	622	13
AA5_34	0.0207	20	0.00069	5	1.46727	1.88659	21	0.282366	15	0.282357	−0.9	0.5	1.27	640	12

Table 1 (*Continued*)

	$^{176}Yb/^{177}Hf$ [a]	±2σ	$^{176}Lu/^{177}Hf$ [a]	±2σ	$^{178}Hf/^{177}Hf$	$^{180}Hf/^{177}Hf$	Sig_{Hf} [b] (V)	$^{176}Hf/^{177}Hf$ [d]	±2σ [c]	$^{176}Hf/^{177}Hf_{(t)}$	εHf(t) [d]	±2σ [c]	T_{DM2} [e] (Ga)	Age [f] (Ma)	±2σ
AA5_37	0.0083	10	0.00023	2	1.46721	1.88645	16	0.282611	16	0.282608	7.9	0.6	0.78	632	13
AA5_38	0.0101	7	0.00031	2	1.46724	1.88664	15	0.282674	20	0.282670	9.4	0.7	0.67	602	11
AA5_42	0.0331	25	0.00097	7	1.46722	1.88654	17	0.282637	20	0.282626	8.7	0.7	0.74	640	15
AA5_43	0.0178	18	0.00057	4	1.46721	1.88665	14	0.282647	18	0.282639	10.2	0.7	0.70	685	15
AA5_44	0.0226	20	0.00070	5	1.46722	1.88668	17	0.282571	18	0.282563	6.7	0.7	0.86	650	13
AA5_45	0.0323	29	0.00111	8	1.46735	1.88690	18	0.282580	20	0.282567	6.1	0.7	0.87	619	12
AA5_46	0.0263	26	0.00079	7	1.46723	1.88650	16	0.282043	20	0.282034	−12.8	0.7	1.91	616	11
AA5_47	0.0194	13	0.00059	4	1.46713	1.88653	17	0.282682	17	0.282675	11.5	0.6	0.63	690	16
AA5_49	0.0130	9	0.00038	2	1.46736	1.88690	15	0.282662	17	0.282657	9.1	0.6	0.70	608	12
AA5_52	0.0316	20	0.00084	5	1.46718	1.88654	19	0.282679	19	0.282669	9.9	0.7	0.66	627	11
AA5_54	0.0261	22	0.00098	10	1.46728	1.88669	18	0.282390	20	0.282378	0.2	0.7	1.22	655	13
AA5_57	0.0725	106	0.00187	27	1.46738	1.88692	13	0.281618	31	0.281545	2.5	1.1	2.24	2052	13
AA5_62	0.0551	52	0.00162	15	1.46720	1.88651	10	0.282674	31	0.282653	11.0	1.1	0.66	699	14
AA5_64	0.0241	21	0.00077	6	1.46721	1.88650	10	0.282512	28	0.282503	4.3	1.0	0.99	638	13
AA5_66b	0.0179	20	0.00053	4	1.46715	1.88648	12	0.282012	20	0.282005	−13.9	0.7	1.96	613	15
AA5_69	0.0337	27	0.00127	10	1.46714	1.88656	6	0.281447	29	0.281393	1.3	1.0	2.46	2229	19
AA5_74	0.0189	14	0.00067	5	1.46730	1.88691	14	0.282576	19	0.282568	7.6	0.7	0.84	685	14
AA5_76	0.0455	30	0.00123	8	1.46727	1.88668	11	0.282439	26	0.282425	0.3	0.9	1.16	583	14
AA5_81	0.0128	10	0.00037	3	1.46721	1.88670	16	0.282677	19	0.282672	11.0	0.7	0.64	671	13
AA5_88	0.0218	22	0.00063	7	1.46722	1.88666	12	0.281188	19	0.281157	1.8	0.7	2.74	2610	14
AA5_90	0.0425	30	0.00126	9	1.46728	1.88677	12	0.282523	22	0.282509	3.4	0.8	0.99	591	14
AA5_98	0.0214	15	0.00067	4	1.46715	1.88663	15	0.282642	18	0.282635	7.9	0.6	0.75	593	10
AA5_102	0.0201	36	0.00062	11	1.46718	1.88667	12	0.282641	21	0.282634	7.7	0.7	0.75	583	19
AA5_107	0.0203	24	0.00065	6	1.46713	1.88644	14	0.282048	22	0.282041	−12.6	0.8	1.90	617	11
AA5_109	0.0241	15	0.00074	5	1.46716	1.88649	16	0.282579	16	0.282570	6.4	0.6	0.86	627	13
AA5_112	0.0513	43	0.00129	9	1.46726	1.88677	16	0.282402	22	0.282386	0.2	0.8	1.21	641	13
AA5_115	0.0167	22	0.00046	6	1.46714	1.88645	15	0.282693	19	0.282686	13.8	0.7	0.57	773	18
AA5_117	0.0260	22	0.00068	6	1.46721	1.88656	14	0.282601	17	0.282593	7.3	0.6	0.81	630	13
AA5_118	0.0232	20	0.00061	5	1.46712	1.88657	14	0.282186	21	0.282179	−7.3	0.7	1.62	633	12
AA5_121	0.0324	23	0.00099	6	1.46712	1.88645	14	0.282596	23	0.282584	7.2	0.8	0.83	638	12
AA5_122	0.0339	26	0.00090	7	1.46717	1.88644	16	0.282693	19	0.282682	10.4	0.7	0.64	629	13
AA5_123	0.0095	10	0.00029	3	1.46713	1.88646	17	0.282672	14	0.282669	10.0	0.5	0.66	633	14
AA6_1	0.0377	48	0.00109	15	1.46712	1.88647	15	0.281586	27	0.281543	3.2	0.9	2.23	2084	15
AA6_4	0.0345	21	0.00103	6	1.46722	1.88665	13	0.282130	25	0.282117	−9.3	0.9	1.74	643	13
AA6_7	0.0318	20	0.00098	6	1.46722	1.88659	13	0.281596	23	0.281558	3.4	0.8	2.21	2068	14
AA6_12	0.0807	65	0.00228	18	1.46719	1.88678	12	0.282024	32	0.281998	−14.2	1.1	1.98	612	8
AA6_13	0.0256	24	0.00087	9	1.46713	1.88645	9	0.281606	25	0.281570	6.2	0.9	2.13	2169	16
AA6_15	0.0353	27	0.00097	7	1.46736	1.88693	11	0.281473	25	0.281434	0.9	0.9	2.41	2152	11
AA6_16	0.0341	39	0.00101	9	1.46717	1.88652	12	0.281582	24	0.281542	3.3	0.9	2.23	2087	16
AA6_23	0.0154	24	0.00046	9	1.46723	1.88648	12	0.281641	23	0.281623	6.8	0.8	2.06	2114	7
AA6_29	0.0310	23	0.00082	6	1.46717	1.88666	12	0.281611	22	0.281577	7.1	0.8	2.11	2198	24
AA6_34	0.0317	56	0.00084	15	1.46729	1.88667	14	0.281581	22	0.281546	6.7	0.8	2.16	2227	11
AA6_35	0.0265	18	0.00075	5	1.46723	1.88667	10	0.282015	24	0.282007	−14.0	0.9	1.96	609	10
AA6_42	0.0448	40	0.00123	10	1.46715	1.88646	13	0.282029	25	0.282015	−13.5	0.9	1.94	619	10
AA6_46	0.0100	13	0.00025	3	1.46728	1.88668	13	0.281582	19	0.281573	3.4	0.7	2.19	2046	10
AA6_52	0.0287	20	0.00081	6	1.46718	1.88668	11	0.281619	21	0.281586	5.5	0.7	2.13	2114	13
AA6_52a	0.0287	20	0.00081	6	1.46718	1.88668	11	0.281619	21	0.281586	5.5	0.7	2.13	2114	13
AA6_83b	0.0329	57	0.00076	13	1.46730	1.88682	15	0.281601	24	0.281572	3.2	0.9	2.19	2039	13
AA6_84	0.0755	158	0.00162	33	1.46725	1.88661	16	0.281598	35	0.281536	1.3	1.2	2.28	2012	17
AA6_85	0.0214	20	0.00058	5	1.46724	1.88675	13	0.281641	22	0.281619	4.6	0.8	2.11	2028	16
AA6_87	0.0392	33	0.00089	8	1.46733	1.88684	17	0.281604	23	0.281569	3.4	0.8	2.19	2054	14
AA6_88	0.0644	42	0.00173	11	1.46727	1.88674	13	0.281615	28	0.281548	2.3	1.0	2.24	2036	23
AA6_90	0.0419	51	0.00105	12	1.46732	1.88693	12	0.281602	28	0.281561	3.2	1.0	2.21	2054	13
AA6_92	0.0641	52	0.00167	13	1.46733	1.88694	11	0.281590	28	0.281525	1.9	1.0	2.28	2054	21
AA6_93	0.0742	85	0.00199	22	1.46721	1.88665	11	0.281622	37	0.281544	2.9	1.3	2.24	2068	13
AA6_96	0.0276	23	0.00076	6	1.46732	1.88674	14	0.281388	29	0.281357	−1.2	1.0	2.55	2180	11
AA6_97	0.0194	46	0.00042	10	1.46728	1.88668	15	0.281574	21	0.281557	4.5	0.7	2.19	2118	15

Table 1 (*Continued*)

	$^{176}Yb/^{177}Hf$ [a]	±2σ	$^{176}Lu/^{177}Hf$ [a]	±2σ	$^{178}Hf/^{177}Hf$	$^{180}Hf/^{177}Hf$	Sig_{Hf} [b] (V)	$^{176}Hf/^{177}Hf$ [d]	±2σ [c]	$^{176}Hf/^{177}Hf_{(t)}$	εHf(t) [d]	±2σ [c]	T_{DM2} [e] (Ga)	Age [f] (Ma)	±2σ
AA6_100	0.0418	44	0.00114	13	1.46712	1.88644	13	0.281605	24	0.281561	2.9	0.8	2.21	2044	16
AA6_103	0.0492	70	0.00122	16	1.46727	1.88668	15	0.281575	26	0.281527	2.9	0.9	2.26	2095	13
AA6_105	0.0297	26	0.00073	6	1.46732	1.88674	14	0.281580	22	0.281552	3.4	0.8	2.22	2076	40
AA6_108	0.0174	27	0.00040	7	1.46727	1.88658	15	0.281575	19	0.281559	4.6	0.7	2.18	2117	23
AA6_111	0.0538	54	0.00143	15	1.46723	1.88652	13	0.281636	26	0.281580	3.5	0.9	2.18	2039	18
AA7_2	0.0364	25	0.00088	6	1.46716	1.88650	13	0.282567	20	0.282557	4.8	0.7	0.91	574	15
AA7_6	0.0330	28	0.00077	6	1.46724	1.88661	14	0.282524	20	0.282516	2.8	0.7	1.00	552	15
AA7_10	0.0313	21	0.00077	5	1.46716	1.88647	15	0.282516	18	0.282508	2.7	0.7	1.01	558	13
AA7_12	0.0425	28	0.00106	7	1.46729	1.88679	12	0.282573	26	0.282562	5.3	0.9	0.89	592	14
AA7_16	0.0369	30	0.00086	7	1.46717	1.88650	15	0.282523	25	0.282514	2.6	0.9	1.00	546	14
AA7_18	0.0416	31	0.00100	7	1.46722	1.88661	13	0.282532	24	0.282522	2.8	0.9	0.99	543	13
AA7_20	0.0248	15	0.00062	4	1.46713	1.88644	10	0.282526	21	0.282520	2.9	0.8	0.99	550	14
AA7_23	0.0428	29	0.00100	7	1.46717	1.88648	16	0.282546	23	0.282535	3.8	0.8	0.95	567	11
AA7_24	0.0464	74	0.00109	14	1.46722	1.88662	15	0.282511	23	0.282499	2.7	0.8	1.02	574	15
AA7_28	0.0703	55	0.00168	12	1.46714	1.88647	18	0.282605	37	0.282586	6.3	1.3	0.84	599	10
AA7_29	0.0542	42	0.00125	8	1.46720	1.88682	18	0.282510	26	0.282497	2.8	0.9	1.02	584	11
AA7_30	0.0672	43	0.00164	11	1.46713	1.88646	13	0.282556	30	0.282539	3.7	1.1	0.95	556	10
AA7_31	0.0826	190	0.00194	36	1.46715	1.88644	12	0.282520	36	0.282499	2.8	1.3	1.02	581	12
AA7_32	0.0297	24	0.00075	6	1.46720	1.88651	12	0.282528	26	0.282520	3.5	0.9	0.98	579	13
AA7_34	0.0371	23	0.00092	6	1.46713	1.88654	15	0.282518	18	0.282508	2.8	0.6	1.01	563	10
AA7_35	0.0871	65	0.00205	16	1.46719	1.88651	12	0.282579	37	0.282557	4.7	1.3	0.91	570	11
AA7_36	0.0528	40	0.00124	8	1.46721	1.88659	19	0.282499	22	0.282485	2.7	0.8	1.04	596	11
AA7_37	0.0343	21	0.00086	5	1.46723	1.88657	14	0.282504	17	0.282495	2.9	0.6	1.02	590	10
AA7_40	0.0529	57	0.00122	12	1.46716	1.88668	16	0.282644	26	0.282629	8.4	0.9	0.75	621	12
AA7_42	0.0803	93	0.00159	15	1.46719	1.88674	18	0.282571	37	0.282553	4.7	1.3	0.91	579	12
AA7_43	0.0616	46	0.00145	10	1.46725	1.88667	15	0.282551	26	0.282536	3.8	0.9	0.95	564	10
AA7_46	0.0923	128	0.00222	27	1.46717	1.88646	12	0.282488	37	0.282465	1.2	1.3	1.09	563	10
AA7_47	0.0399	45	0.00090	11	1.46718	1.88656	18	0.281642	31	0.281607	4.4	1.1	2.13	2037	15
AA7_48	0.0336	24	0.00083	6	1.46731	1.88691	11	0.282538	20	0.282529	3.5	0.7	0.97	561	11
AA7_49	0.0440	27	0.00109	8	1.46714	1.88650	12	0.282523	26	0.282512	2.6	0.9	1.01	552	10
AA7_52	0.0287	26	0.00071	6	1.46722	1.88657	14	0.282529	21	0.282521	3.1	0.7	0.99	556	11
AA7_53	0.0607	80	0.00145	16	1.46716	1.88670	13	0.282490	27	0.282474	2.1	1.0	1.07	586	12
AA7_56	0.0735	45	0.00156	10	1.46714	1.88661	15	0.282537	28	0.282521	3.1	1.0	0.99	557	11
AA7_57	0.0701	52	0.00148	11	1.46713	1.88646	15	0.282563	27	0.282548	4.0	1.0	0.93	555	10
AA7_59	0.0530	35	0.00129	8	1.46726	1.88670	11	0.282540	24	0.282527	3.2	0.8	0.98	554	10
AA7_60	0.0325	22	0.00078	5	1.46724	1.88670	13	0.282253	42	0.282245	−6.6	1.5	1.52	560	16
AA7_60	0.0397	50	0.00098	14	1.46716	1.88657	15	0.281641	62	0.281601	6.1	2.2	2.10	2121	17
AA7_61	0.2873	448	0.00495	74	1.46715	1.88646	14	0.282630	100	0.282576	5.7	3.5	0.87	585	11
AA7_63	0.0485	39	0.00103	8	1.46724	1.88686	15	0.282509	22	0.282498	2.8	0.8	1.02	580	12
AA7_64	0.0507	49	0.00126	13	1.46721	1.88653	13	0.282548	25	0.282535	3.2	0.9	0.96	540	11
AA7_68	0.0193	14	0.00051	3	1.46712	1.88647	11	0.282515	19	0.282510	2.7	0.7	1.01	556	13
AA7_70	0.0404	26	0.00102	6	1.46725	1.88662	15	0.282506	19	0.282495	2.0	0.7	1.04	548	12
AA7_73	0.0357	22	0.00091	6	1.46718	1.88657	14	0.282508	20	0.282498	2.0	0.7	1.04	544	10
AA7_75	0.0620	66	0.00157	18	1.46723	1.88657	12	0.282531	25	0.282515	2.6	0.9	1.00	543	10
JMC475, $n = 14$		–	–	–	1.46716	1.88667	19	0.282146	9						
GJ-1, $n = 23$	0.0100	16	0.00031	2	1.46723	1.88666	11	0.282006	22	0.282003	−13.9	0.8	2.18	606	4
Ples., $n = 18$	0.0072	19	0.00019	6	1.46722	1.88666	22	0.282489	16	0.282489	−2.6	0.6	1.35	338	2

[a] $^{176}Yb/^{177}Hf = (^{176}Yb/^{173}Yb)_{true} \times (^{173}Yb/^{177}Hf)_{meas} \times (M_{173(Yb)}/M_{177(Hf)})^{\beta(Hf)}$. The $^{176}Lu/^{177}Hf$ were calculated in a similar way by using the $^{175}Lu/^{177}Hf$. Quoted uncertainties (absolute) relate to the last quoted figure. The effect of the inter-element fractionation on the Lu/Hf was estimated to be about 6% or less based on analyses of the GJ-1 and Plesovice zircons.

[b] Mean Hf signal in volt.

[c] Uncertainties are quadratic additions of the within-run error and the daily reproducibility of the 40 ppb JMC475 solution. Uncertainties for the JMC475, GJ-1 and Plesovice are 2SD.

[d] Initial $^{176}Hf/^{177}Hf$ and εHf calculated using the age determined by LA-ICP-MS dating (see last two rows).

[e] Two stage model age in billion years using the measured $^{176}Lu/^{177}Lu$ of each spot (first stage = age of zircon), a value of 0.0113 for the average continental crust (second stage), and a juvenile crust $^{176}Lu/^{177}Lu$ and $^{176}Hf/^{177}Hf$ of 0.0384 and 0.28314, respectively (see Dhuime et al., 2011; Gerdes and Zeh, 2006 for details and references).

[f] U-Pb LA-ICP-MS age and error.

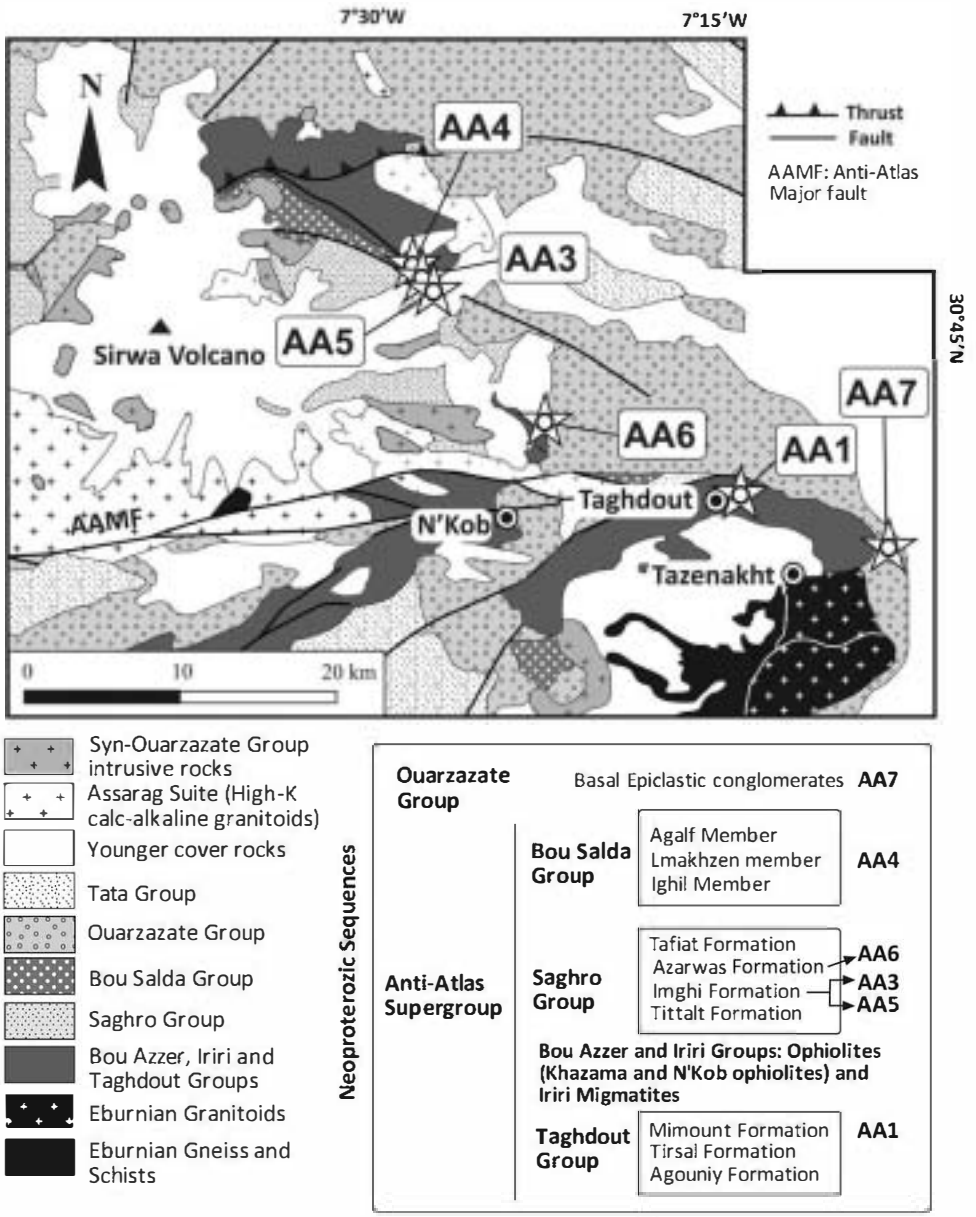

Fig. 2. Simplified geological map and stratigraphic sketch column of the Sirwa Window (Modified after Thomas et al., 2002) showing the location of the samples and their relative position.

group with positive εHf_i forms a rough linear array nearly parallel to the $^{176}Lu/^{177}Hf$ evolution of a continental crust extracted from the depleted mantle during the Pan-African cycle (Fig. 3b). Zircons with values closets to the depleted mantle array have ages between 620 and 720 Ma, consistent with the formation of juvenile crust in an early island-arc setting. Zircon with ages of 600–550 have somewhat lower εHf_i suggesting that juvenile magmas where contaminated by older crust or recycling of the juvenile island arcs together with some older crust. Both scenarios are compatible with a continental arc setting. Negative εHf_i values occur mainly in the interval 590–650 Ma. A group of 10 zircons with the lowest negative εHf_i, between −10 and −15 and T_{DM} model ages between 1.85 and 2.0 Ga can be explained by almost pure reworking of older Eburnian crust, while the relatively numerous group with negative intermediate values are only compatible with mixing of the Eburnian and the newly formed juvenile crust (Fig. 3a and b). As the formation of juvenile crust is the main magmatic process expected in an arc environment, the predominance of a juvenile Hf isotope signature suggests an island arc and a continental arc as most likely origin for the magmas from which the detrital zircons derived from. Although Neoproterozoic zircons from the Anti-Atlas Supergroup form a coherent group (Fig. 3b) some differences related to stratigraphic position can be highlighted. Samples AA3 and AA5 have different εHf, with a tendency to positive values in AA5 and negative in AA3, despite they belong to the same formation (Fig. 2). This fact can be probably explained because AA3 is a diamictite, with a potential for containing ice-rafted debris which could be far-traveled.

Zircons of Neoproterozoic age are present in all the samples, except in the oldest passive margin Taghdout quartzite (AA1). Going to the top of the sedimentary sequence, the proportion of Neoproterozoic zircons in each sample is 80% (AA5), 52% (AA3), 7% (AA6), 5% (AA4) and 97% (AA7), being the youngest zircon population 610–620 Ma. Abati et al. (2010) proposed that this young zircon

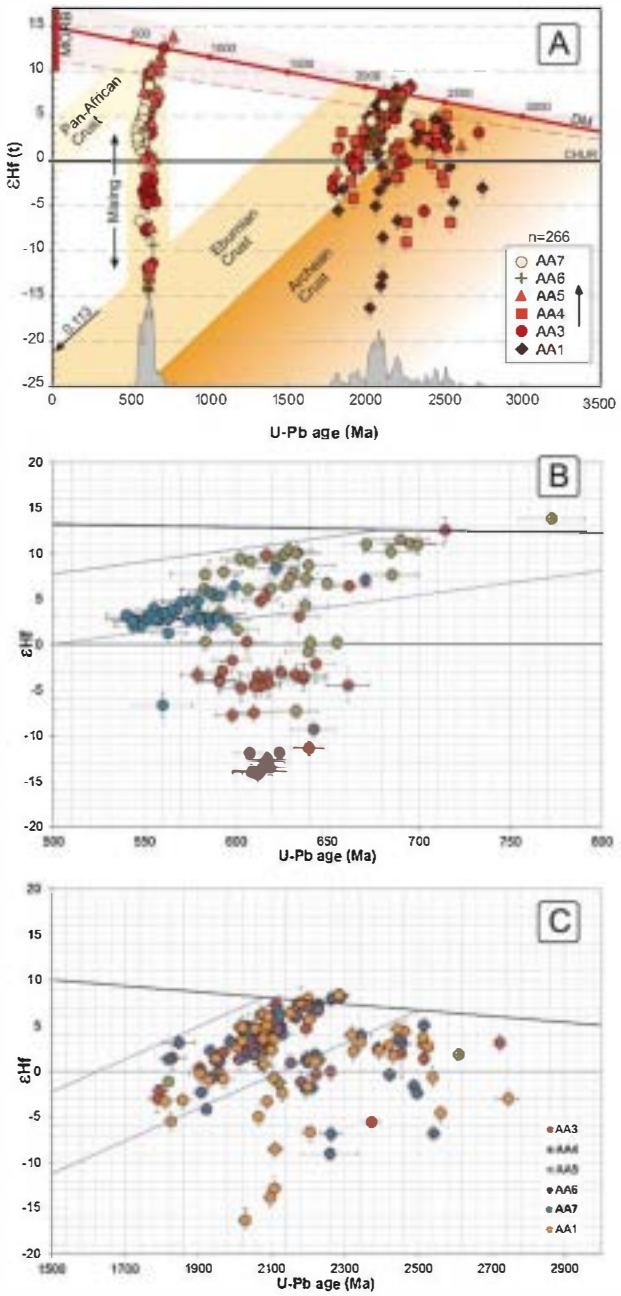

Fig. 3. (a) Hf isotope evolution diagram summarizing the data of zircon from all the rocks studied. The continental crust evolution trends of the main components of the WAC are shown in different colors, and the probability plot of the zircon age populations are represented in grey. See text for discussion. For details and references of depleted mantle evolution see Gerdes and Zeh (2006) and Dhuime et al. (2011). (b) Hf isotope evolution diagram for the "young" (Neoproterozoic zircons). (c) Hf isotope evolution diagram for the "old" zircons. Data were calculated using the decay constant of 1.867×10^{-11} (Scherer et al., 2001), and the CHUR parameters of Bouvier et al. (2008).

group is related with the evolution and dismantling of an ensialic magmatic arc built upon the continental margin of the WAC. The new data presented here strongly support that interpretation. All these features fit well with an origin in a ensialic magmatic arc geodynamic setting, which in turn fits with the general geodynamic scenario of the north Gonwana margin for this age, dominated by a well-documented Neoproterozoic magmatic arc activity (*e.g.* Nance et al., 2008 and references therein).

4.2. *Juvenile crust formation at ca. 2.3–2.1 Ga*

One of the major crustal growth events identified in the WAC is the Eburnian orogeny (*e.g.* Abouchami et al., 1990). Medium to high grade metamorphic rocks cross-cut by Eburnian (*ca.* 2.2–2.0 Ma) granitoid batholiths outcrop in several inliers in the Anti-Atlas and form a great part of the Reguibat and Man Shields (Fig. 1a). Geochemical and Nd isotopic studies in the Zenaga Inlier of the Anti-Atlas suggest a juvenile metasedimentary crustal source for some peraluminous granitoids, although the geochemical signature of some parts of the plutons seems strongly modified by a fluid-related reactivation during the Pan-African orogeny (Ennih and Liegeois, 2008). In the studied samples, the zircons of the age interval 2.3–1.7 Ga represent a proportion with respect to the total population between 93% (sample AA6, sandstone from Azarwas formation) and 3% in the younger sample (AA7, Ouarzazate group conglomerate). The Hf isotope data of this study confirm the predominantly juvenile origin of the Eburnian rocks, with only minor components of Archean crust involved. About 75% of the 154 analyzed grains have positive εHf_i values. Zircons with positive to slightly negative εHf_i in the age interval 1.7–2.3 Ga arrange in a linear array with a slope of $^{176}Lu/^{177}Hf$ of ~0.01 suggesting a main phase of crustal growth between 2.3 and 2.1 Ga and subsequent recycling of this crust between 2.2 and 1.8 Ga (Fig. 3a and c). This εHf_i-age evolution is consistent with formation of juvenile magmas in an island arc setting, the changeover to a continental arc setting and a subsequent continent-continent collision. While during the first stage only juvenile magmas extracted from a depleted mantle reservoir were formed, the subsequent stages are characterized by increasing amount of reworking of the earlier arc rocks and older crustal components.

Consequently, the evolution of the Eburnian orogeny is apparently dominated by new crustal formation in a magmatic arc environment. The Archean component involved in the Eburnian cycle is revealed by the zircons with negative εHf_i values, with T_{DM} model ages varying between 2.25 and 3.26 Ga. The small size of the group of zircons with the lowest εHf_i suggest that only limited amounts of old Mesoarchean crust (between 3.25 and 3.0) were reworked during the Eburnian cycle, and the zircons with intermediate epsilon values indicate mixing of the Archean precursors with variable amounts of the Eburnian arc rocks.

4.3. *Lower Paleoproterozoic and Neoarchean evolution (2.3–2.75 Ga)*

The oldest group of zircons, between 2.3 and 2.75 Ga, is form a minor age population represented in all samples except in AA6 and AA7. They are a small proportion in samples AA3 and AA5 (1% and 5%), whereas they reach a significant proportion, 17% and 16%, in samples AA1 and AA4, respectively (Fig. 3a). The meaning of these ages is not clear, because no tectonothermal events in that range of ages have been described in the WAC up to now (except for the older part of the range). The youngest granitoids related with the Neoarchean development of the Reguibat shield are 2726 ± 7 Ma (Potrel et al., 1998; Key et al., 2008), and the following registered events are the early Eburnian *ca.* 2.25 Ga. A gap in zircon ages between *ca.* 2.7 and 2.2 Ga is assumed to be characteristic of rocks coming from the WAC (Nance et al., 2008). Abati et al. (2010) suggested that the presence of this group of zircons in these rocks indicates that there could be a tectonothermal event in the northern part of the WAC with a peak at *ca.* 2.5–2.4 Ga, which has not been described yet. The Hf model ages of this zircons lie between 2.38 and 3.16 Ga, and 75% of εHf_i values are positive. Although the values are not so close to the depleted mantle array than those of the previous group, their main isotopic component is also juvenile, mixed with variable proportions of reworked Archean crust. Thus,

this hypothetic event can be associated with reworking of a juvenile crust with only moderate amounts of Archean crust involved. Other possibility is that this group of zircons is far-traveled and come from an unknown source, but at this respect only speculations can be made.

5. Summary and conclusions

The Hf isotope record of detrital zircons from Neoproterozoic sequences of the Anti-Atlas gives some clues about the nature of the major geologic events forming the WAC and their crustal evolution. Three major groups of zircon ages point to the existence of three peaks of TTG production. The three groups have predominant juvenile signatures, and their T_{DM} ages indicate the moment of extraction of crustal domains from the mantle. Other isotopic components suggest variable amounts of reworking of older crust:

1. The Pan-African evolution is dominated by juvenile crust formation, as is suggested by the high proportion of zircons with positive epsilon values (more than 70%). The juvenile character is linked with the evolution of a magmatic arc developed in the north margin of the WAC, identified with the long-lived Cadomian–Avalonian arc activity of the North Gondwana margin. Reworking of the Eburnian crust is indicated by zircons with low εHf_i values and T_{DM} ages between 1.85 and 2.0 Ga and interaction and mixing between this old crust and the juvenile magmas is indicated by zircons with intermediate epsilon and T_{DM} ages.
2. The major crustal growth event of 2.3–2.1 Ga typical of the WAC also involves predominance of juvenile crust formation, mixed with variable proportions of reworked Archean crust. The εHf_i-age evolution is consistent with a first magmatic episode in an island arc setting, the changeover to a continental arc setting and a subsequent continent-continent collision.
3. The Lower Paleoproterozoic and Neoarchean evolution involves a group of detrital zircon ages (described by Abati et al., 2010) that has not been identified in the igneous or metamorphic rocks of the north WAC basement. Their Hf isotope signature points to reworking of juvenile crust mixed with moderate amounts of Archean crust. The significance of these ages is uncertain: they can represent a tectonothermal event not discovered yet in the Reguibat Shield or the zircons can be far traveled from an unknown source.

Acknowledgements

Field work was funded by project A-7287-06 from the Agencia Española de Cooperación Internacional (AECI), and analytical work was funded by project CM-UCM-910129 from the Comunidad de Madrid.

Appendix A. Supplementary data

Supplementary data associated with this article can be found, in the online version, at http://dx.doi.org/10.1016/j.precamres.2012.06.005.

References

Abati, J., Arenas, R., Martínez Catalán, J.R., Díaz García, F., 2003. Anticlockwise P-T path of granulites from the Monte Castelo Gabbro (Ordenes Complex NW Spain). Journal of Petrology 44 (2), 305–327.

Abati, J., Aghzer, A.M., Gerdes, A., Ennih, N., 2010. Detrital zircon ages of Neoproterozoic sequences of the Moroccan Anti-Atlas belt. Precambrian Research 181 (1–4), 115–128.

Abouchami, W., Boher, M., Michard, A., Albarede, F., 1990. A major 2.1 Ga event of mafic magmatism in West Africa: an early stage of crustal accretion. Journal of Geophysical Research 95, 17605–17629.

Aït Malek, H., Gasquet, D., Bertrand, J.M., Leterrier, J., 1998. Eburnian and Panafrican granitoids from the Igherm, Kerdous and Bas-Draa Proterozoic inliers (western Anti-Atlas, Morocco): U-Ph geochronology on zircon. Comptes Rendus de l'Academie des Sciences Series IIA Earth and Planetary Science 327, 819–826.

Amelin, Y., Lee, D.C., Halliday, A.N., 2000. Early-middle archaean crustal evolution deduced from Lu-Hf and U-Pb isotopic studies of single zircon grains. Geochimica et Cosmochimica Acta 64 (24), 4205–4225.

Andersen, T., Griffin, W.L., Pearson, N.J., 2002. Crustal evolution in the SW part of the baltic shield: the Hf isotope evidence. Journal of Petrology 43 (9), 1725–1747.

Auvray, B., Peucat, J.-J., Potrel, A., Burg, J.-P., Caruba, C., Dars, R., Lo, K., 1992. Données géochronologiques nouvelles sur l'Archéen de l'Amsaga (Dorsale Réguibat Mauritanie). Comptes Rendus de l'Académie des Sciences 315 (1), 63–70.

Boher, M., Abouchami, W., Michard, A., Albarede, F., Arndt, N.T., 1992. Crustal growth in West Africa at 2.1 Ga. Journal of Geophysical Research 97, 345–369.

Bouvier, A., Vervoort, J.D., Patchett, P.J., 2008. The Lu-Hf and Sm-Nd isotopic composition of CHUR: constraints from unequilibrated chondrites and implications for the bulk composition of terrestrial planets. Earth and Planetary Science Letters 273 (1–2), 48–57.

De Wall, H., Kober, B., Greiling, R.O., Errami, E., Ennih, N., 2001. Age and structural setting of the grantoid emplacement in the area of Imiter (Eastern Saghro). In: Abstrac, 2nd Coll. 3M, Marrakech, p. 19.

Dhuime, B., Hawkesworth, C., Cawood, P., 2011. When continents formed. Science 331 (6014), 154–155.

D'Lemos, R.S., Inglis, J.D., Samson, S.D., 2006. A newly discovered orogenic event in Morocco: Neoproterozic ages for supposed Eburnean basement of the Bou Azzer inlier" Anti-Atlas Mountains. Precambrian Research 147 (1–2), 65–78.

El Hadi, H., Simancas, J.F., Martínez-Poyatos, D., Azor, A., Tahiri, A., Montero, P., Fanning, C.M., Bea, F., González-Lodeiro, F., 2010. Structural and geochronological constraints on the evolution of the Bou Azzer Neoproterozoic ophiolite (Anti-Atlas, Morocco). Precambrian Research 182 (1–2), 1–14.

Ennih, N., Liegeois, J.-P., 2008. The boundaries of the West African craton, with special reference to the basement of the Moroccan metacratonic Anti-Atlas belt. Geological Society, London, Special Publications 297 (1), 1–17.

Frei, D., Gerdes, A., 2009. Precise and accurate in situ U-Pb dating of zircon with high sample throughput by automated LA-SF-ICP-MS. Chemical Geology 261 (3–4), 261–270.

Gasquet, D., Levresse, G., Cheilletz, A., Azizi-Samir, M.R., Mouttaqi, A., 2005. Contribution to a geodynamic reconstruction of the Anti-Atlas (Morocco) during Pan-African times with the emphasis on inversion tectonics and metallogenic activity at the Precambrian–Cambrian transition. Precambrian Research 140 (3–4), 157–182.

Gasquet, D., Ennih, N., Liégeois, J.P., Soulaimani, A., Michard, A., 2008. The Pan-African Belt. Continental Evolution: The Geology of Morocco, pp. 33–64.

Gerdes, A., Zeh, A., 2006. Combined U-Ph and Hf isotope LA-(MC-)ICP-MS analyses of detrital zircons: comparison with SHRIMP and new constraints for the provenance and age of an Armorican metasediment in Central Germany. Earth and Planetary Science Letters 249 (1–2), 47–61.

Gerdes, A., Zeh, A., 2009. Zircon formation versus zircon alteration–new insights from combined U-Ph and Lu-Hf in situ LA-ICP-MS analyses, and consequences for the interpretation of Archean zircon from the Central Zone of the Limpopo Belt. Chemical Geology 261 (3–4), 230–243.

Griffin, W.L., Belousova, E.A., Shee, S.R., Pearson, N.J., O'Reilly, S.Y., 2004. Archean crustal evolution in the northern Yilgarn Craton: U-Ph and Hf-isotope evidence from detrital zircons. Precambrian Research 131 (3–4), 231–282.

Hefferan, K.P., Admou, H., Karson, J.A., Saquaque, A., 2000. Anti-Atlas (Morocco) role in Neoproterozoic Western Gondwana reconstruction. Precambrian Research 103, 89–96.

Hirdes, W., Davis, D.W., Eisenlohr, B.N., 1992. Reassessment of Proterozoic granitoid ages in Ghana on the basis of U/Ph zircon and monazite dating. Precambrian Research 56 (1–2), 89–96.

Hurley, P.M., Leo, G.W., White, R.W., Fairbairn, H.W., 1971. Liberian age province (about 2700 m.y.) and adjacent provinces in Liberia and Sierra Leone. Geological Society of America Bulletin 82 (12), 3483–3490.

Inglis, J.D., MacLean, J.S., Samson, S.D., D'Lemos, R.S., Admou, H., Hefferan, K., 2004. A precise U-Pb zircon age for the Bleïda granodiorite, Anti-Atlas, Morocco: implications for the timing of deformation and terrane assembly in the eastern Anti-Atlas. Journal of African Earth Sciences 39 (3–5), 277–283.

Janousek, V., Gerdes, A., Vrana, S., Finger, F., Erban, V., Friedl, G., Braithwaite, C.J.R., 2006. Low-pressure Granulites of the Lisov Massif, Southern Bohemia: Visean Metamorphism of Late Devonian Plutonic Arc Rocks. J. Petrology 47 (4), 705–744.

Key, R.M., Loughlin, S.C., Gillespie, M., Del Rio, M., Horstwood, M.S.A., Crowley, Q.G., Darbyshire, D.P.F., Pitfield, P.E.J., Henney, P.J., 2008. Two mesoarchaean terranes in the Reguibat shield of NW Mauritania. Geological Society, London, Special Publications 297 (1), 33–52.

Kröner, A., Ekwueme, B.N., Pidgeon, R.T., 2001. The oldest rocks in West Africa: SHRIMP zircon age for early archean migmatitic orthogneiss at Kaduna, Northern Nigeria. The Journal of Geology 109 (3), 399–406.

Leblanc, M., Lancelot, J.R., 1980. Interprétation géodynamique du domaine panafricain (Précambrien terminal) de l'Anti-Atlas (Maroc) à partir de données géologiques et géochronologiques. Canadian Journal of Earth Sciences 17 (1), 142–155.

Levresse, G., Azizi, M.S., Cheilletz, A., Gasquet, D., Zyadi, R., Ennaciri, D., Archibald, D., Ouguir, H., 2001. Le gisement Ag–Hg d'Imiter (Anti-Atlas, Maroc): Nouvelles donneés U-Ph, $^{40}Ar/^{39}Ar^{*34}S$ et microstructurales appuyant le modèle génétique hydrothermal-épithermal. In: Abstract 2nd Coll. 3M, Marrakech, p. 97.

Liégeois, J.P., Claessens, W., Camara, D., Klerkx, J., 1991. Short-lived Eburnian orogeny in southern Mali. Geology, tectonics, U-Pb and Rb-Sr geochronology. Precambrian Research 50 (1–2), 111–136.

Morag, N., Avigad, D., Gerdes, A., Belousova, E., Harlavan, Y., 2011. Crustal evolution and recycling in the northern Arabian-Nubian shield: new perspectives from zircon Lu-Hf and U-Pb systematics. Precambrian Research 186 (1–4), 101–116.

Nance, R.D., Murphy, J.B., Strachan, R.A., Keppie, J.D., Gutierrez-Alonso, G., Fernandez-Suarez, J., Quesada, C., Linnemann, U., D'lemos, R., Pisarevsky, S.A., 2008. Neoproterozoic-early Palaeozoic tectonostratigraphy and palaeogeography of the peri-Gondwanan terranes: Amazonian v. West African connections. Geological Society, London, Special Publications 297 (1), 345–383.

Nebel-Jacobsen, Y., Münker, C., Nebel, O., Gerdes, A., Mezger, K., Nelson, D.R., 2010. Reworking of Earth's first crust: constraints from Hf isotopes in Archean zircons from Mt. Narryer, Australia. Precambrian Research 182 (3), 175–186.

Patchett, P.J., Kouvo, O., Hedge, C.E., Tatsumoto, M., 1982. Evolution of continental crust and mantle heterogeneity: evidence from Hf isotopes. Contributions to Mineralogy and Petrology 78 (3), 279–297.

Potrel, A., Peucat, J.J., Fanning, C.M., Auvray, B., Burg, J.P., Caruba, C., 1996. 3.5 Ga old terranes in the West African Craton, Mauritania. Journal of the Geological Society 153 (4), 507–510.

Potrel, A., Peucat, J.J., Fanning, C.M., 1998. Archean crustal evolution of the West African Craton: example of the Amsaga Area (Reguibat Rise) U-Pb and Sm-Nd evidence for crustal growth and recycling. Precambrian Research 90, 107–117.

Rocci, G., Bronner, G., Deschamps, M. (Eds.), 1991. Crystalline Basement of the West African Craton. The West African Orogens and Circum-Atlantic Correlatives. Springer-Verlag, Berlin, pp. 31–61.

Samson, S.D., Inglis, J.D., D'Lemos, R.S., Admou, H., Blichert-Toft, J., Hefferan, K., 2004. Geochronological, geochemical, and Nd-Hf isotopic constraints on the origin of Neoproterozoic plagiogranites in the Tasriwine ophiolite, Anti-Atlas orogeny, Morocco. Precambrian Research 135 (1–2), 133–147.

Saquaque, A., Admou, H., Karson, J., Hefferan, K., Reuber, I., 1989. Precambrian accretionary tectonics in the BouAzzer-El Graara region, Anti-Atlas, Morocco. Geology 17 (12), 1107–1110.

Scherer, E., Münker, C., Mezger, K., 2001. Calibration of the Lutetium–Hafnium clock. Science 293 (5530), 683–687.

Schofield, D.I., Horstwood, M.S.A., Pitfield, P.E.J., Crowley, Q.G., Wilkinson, A.F., Sidaty, H.C.O., 2006. Timing and kinematics of Eburnean tectonics in the central Reguibat shield, Mauritania. Journal of the Geological Society 163 (3), 549–560.

Stevenson, R.K., Patchett, P.J., 1990. Implications for the evolution of continental crust from Hf isotope systematics of Archean detrital zircons. Geochimica et Cosmochimica Acta 54 (6), 1683–1697.

Thiéblemont, D., Goujou, J.C., Egal, E., Cocherie, A., Delor, C., Lafon, J.M., Fanning, C.M., 2004. Archean evolution of the Leo Rise and its Eburnean reworking. Journal of African Earth Sciences 39 (3–5), 97–104.

Thomas, R.J., Chevallier, L.P., Gresse, P.G., Harmer, R.E., Eglington, B.M., Armstrong, R.A., de Beer, C.H., Martini, J.E.J., de Kock, G.S., Macey, P.H., Ingram, B.A., 2002. Precambrian evolution of the Sirwa Window, Anti-Atlas Orogen, Morocco. Precambrian Research 118 (1–2), 1–57.

Walsh, G.J., Aleinikoff, J.N., Benziane, F., Yazidi, A., Armstrong, T.R., 2002. U-Pb zircon geochronology of the Paleoproterozoic Tagragra de Tata inlier and its Neoproterozoic cover, western Anti-Atlas, Morocco. Precambrian Research 117, 1–20.

Zhang, S.-B., Zheng, Y.-F., Wu, Y.-B., Zhao, Z.-F., Gao, S., Wu, F.-Y., 2006. Zircon U-Pb age and Hf isotope evidence for 3.8 Ga crustal remnant and episodic reworking of Archean crust in South China. Earth and Planetary Science Letters 252 (1–2), 56–71.